TRANSIENT VIBRATION IN A SIMPLE FLUID CARRYING PIPE SYSTEM

Nicholas Steens and Jie Pan[1]
School of Mechanical Engineering, The University of Western Australia, Perth, Western Australia
1. pan@mech.uwa.edu.au

ABSTRACT: This study aimed to investigate the behaviour of coupled transient acoustic and structural waves travelling within an L-shaped, statically pressurised, water filled pipe system consisting of two pipe straights separated by a pipe bend. Specifically, theoretical models were utilised to predict the time domain response of the system subject to a single, impulse-like excitation applied to a boundary modelled as an end cap. Two models of the bend were used: one utilised a simple discrete model and the other a more complicated continuous model. Moreover, an experimental rig was designed and built to test the theory. The designed ring frequency and ratio of bend radius to pipe radius were respectively 24 kHz and 4.4. The results show that for a broad impulse consisting of significant frequencies up to 1 kHz, the discrete bend model is superior to the continuous model due to computational efficiency.

1. INTRODUCTION

Despite many decades of research, transient vibration within fluid carrying pipe systems still presents vibration and dynamic fatigue problems in industry. In order to move forward, the limitations of current methods and models need to be more rigorously assessed. This is the background motivation for this study.

Preliminary research into 'water-hammer' dates back to pre-1900s. After the 1960s, much of the work in this particular field of fluid-structure interaction ("FSI") focused on modelling low frequency response in conjunction with the various forms of coupling. D'Souza and Oldenburger's work [1] was one of the first studies to analyse pressure waves in a straight pipe interacting with a closed end. The theoretical work utilised Laplace transformations, concentrated on frequencies less than 100 Hz and took account of frictional coupling. Davidson and Smith [2] were the first to model bends in a Timoshenko-like manner but without Poisson and frictional coupling. They analysed an L-shaped system in the frequency domain. They solved the partial differential equations analytically by a series approximation to obtain a bend transfer matrix. They validated their analysis with mobility experiments. Davidson and Samsury [3] extended the analysis of Davidson & Smith and analysed a system incorporating one in-plane and one out-of-plane bend. The results of these two papers are further discussed in the comparison paper by Hatfield et al. [4]. In their paper the configurations from both of the previous Davidson papers are solved using a component-synthesis method and the former PDE series approximation method.

With regard to the modelling of pipe bends, Wood and Chao [5] conducted time domain experimental work on various bend set-ups and showed that rigidly supported bends had little influence on pressure waves, but unsupported bends affected the fluid considerably. Their experimental work was thorough and consisted of a series of tests involving 30˚, 60˚, 90˚, 120˚ and 150˚ mitred bends. Wilkinson [6] in his frequency domain analysis was the first to present a complete fourteen equation pipe straight model which accounted for all the important wave families (pressure, axial, flexural and torsional) in low frequency systems. He utilised the transfer matrix method in which pipe bends were modelled as a series of two point discontinuities and mitred straight pipe segments. All straight segments were modelled by the Bernoulli-Euler model and did not take into account Poisson coupling. Like Davidson and his co-authors, Valentin *et al.* [7] also analysed a Timoshenko pipe bend model in an L-shaped system, but unlike the former, they took into account Poisson coupling. Lesmez *et al*. [8] used Wilkinson's transfer matrix method except that they use the fourteen equation model.

The work of Tijsseling *et al*. [9] provided many useful benefits to this study. They use the method-of-characteristics to solve a subset of the fourteen equation model for an L-shaped pipe in the time domain. They present simple boundary conditions and a discrete model of the pipe neglecting both the size and mass of the bend. Additionally, they attempt to model cavitation and in doing so provide a useful insight into the effects and potential occurrence of the phenomenon. Experimentally, they excite the system by impacting one end of the pipe with a large, pendulum-like rod. They also experimentally investigate the effect of statically pressurizing the fluid prior to impact in order to prevent the occurrence of cavitation. The study by Vardy *et al.* [10] is similar to that above but analyses a T-piece pipe system instead.

In this study, a subset of the fourteen-equation model (eight equations) is used to model the pipe straights and two models are used to model the pipe bend: (1) a simple discrete model from Tijsseling *et al.* [9] which neglects the geometry and mass of the bend and (2) a more complicated model from Valentin *et al.* [7]. The former was tested without consideration to the input frequency while the latter has not yet been tested experimentally. It is the aim of this study to compare predictions by both bend models in the time domain with time domain histories taken from a well controlled experiment.

1. THEORY

Theoretical Models

The fluid in the system is assumed to be homogeneous, isotropic and perfectly elastic. No dissipative effects occur and density changes are small. There is also assumed to be an absence of liquid column separation. Lastly and most importantly, the fluid wave is assumed to be planar or one-dimensional in the direction of the pipe axial axis.

In terms of the structure, it is assumed that the pipe material is linearly elastic and damping is negligible. The pipe's axial response is based on the membrane model and because of the coupling with the internal fluid, the radial pipe motion is quasi-static and a biaxial stress state results in which the radial stress is zero. Furthermore, the transverse response is modelled as a beam. For the continuous pipe bend, the equations for these two models are coupled. For the pipe straight, they are not.

The lateral pipe motion is governed by the Timoshenko model. Unlike the simpler Euler-Bernoulli beam model, this accounts for both rotary inertia and deformation due to shear forces. Like the fluid, the structural waves are assumed to be planar. Additionally, changes in the angle of the bend and their associated effects on the wave dynamics are assumed negligible; elbow ovalization and the associated increase in flexibility and stress intensification are ignored.

In terms of the discrete model, it neglects the mass and the dimensions of the bend as well as the forces exerted on the bend due to changes in fluid momentum. This model is valid if the length of the bend is considerably smaller than that of the straight pipes connected to it. Moreover, like the continuous model, the bend angle is assumed to remain constant. To account for the loss of the pipe length, half of the actual centerline length of the bend is added onto each pipe straight.

The continuous pipe bend model consists of Equations (1) – (8). The pipe straight model can be obtained from these equations by setting $R_b \approx \infty$ (with a change in coordinate system also, see Figure 2). Note that V is the centerline fluid velocity, P the fluid pressure, ρ_f the fluid density, (s, n, r) is the coordinate system, R_b the bend radius, R_p the internal pipe radius, K the fluid bulk modulus, υ the Poisson's ratio, E the Young's modulus for the pipe material, T the pipe wall thickness, t the time, $\dot{u}_s$ the axial pipe velocity, $\dot{u}_r$ the transverse pipe velocity, ρ_p the pipe material density, σ_s the axial pipe stress ($N_s = A_p\sigma_s$), A_p the pipe cross-sectional area, Q_r the pipe shear force, κ the Timoshenko shear coefficient, G the shear modulus, $\dot{\theta}_n$ the rotation of the pipe element cross-sectional face, A_f the fluid cross-sectional area, I_p the second moment of area of the pipe and M_n the pipe moment.

Note that $\phi = \partial u_r/\partial s$ and is the rotation of the pipe element cross-sectional face $s + ds$, ξ is the pipe element centre-line rotation loss at $s + ds$ due to shear, $\xi = Q_r/\kappa GA_p$ and that the rotation of the centre line of the element is $\theta_n = -(\phi + \xi - u_s/R_b)$.

$$\frac{\partial V}{\partial t} + \frac{1}{\rho_f}\frac{\partial P}{\partial s} = 0 \tag{1}$$

$$2\frac{R_b^2}{R_p^2}\left[1-\left(1-\frac{R_p^2}{R_b^2}\right)^{\frac{1}{2}}\right]\frac{\partial V}{\partial s} + \left(\frac{1}{K} + \frac{2R_p(1-\nu^2)}{ET}\right)\frac{\partial P}{\partial t} - \frac{2\upsilon}{E}\frac{\partial \dot{u}_s}{\partial s} + (1-2\upsilon)\frac{\dot{u}_r}{R_p} = 0 \tag{2}$$

$$\frac{\partial \dot{u}_s}{\partial t} - \frac{1}{\rho_p}\frac{\partial \sigma_s}{\partial s} - \frac{1}{A_p R_b}Q_r = 0 \tag{3}$$

$$\frac{\partial \dot{u}_s}{\partial s} - \frac{1}{E}\frac{\partial \sigma_s}{\partial t} + \frac{\upsilon R_p}{ET}\frac{\partial P}{\partial t} + \frac{\dot{u}_r}{R_b} = 0 \tag{4}$$

$$\frac{\partial \dot{u}_r}{\partial s} + \frac{1}{\kappa GA_p}\frac{\partial Q_r}{\partial t} - \frac{\dot{u}_s}{R_b} = -\dot{\theta}_n \tag{5}$$

$$\frac{\partial \dot{u}_r}{\partial t} + \frac{1}{\rho_p A_p + \rho_f A_f}\left[\frac{\partial Q_r}{\partial s} + \frac{A_p}{R_b}\sigma_s - \frac{A_f}{R_b}P\right] = 0 \tag{6}$$

$$\frac{\partial \dot{\theta}_n}{\partial s} + \frac{1}{EI_p}\frac{\partial M_n}{\partial t} = 0 \tag{7}$$

$$\frac{\partial \dot{\theta}_n}{\partial t} + \frac{1}{\rho_p I_p}\frac{\partial M_n}{\partial s} = \frac{Q_r}{\rho_p I_p} \tag{8}$$

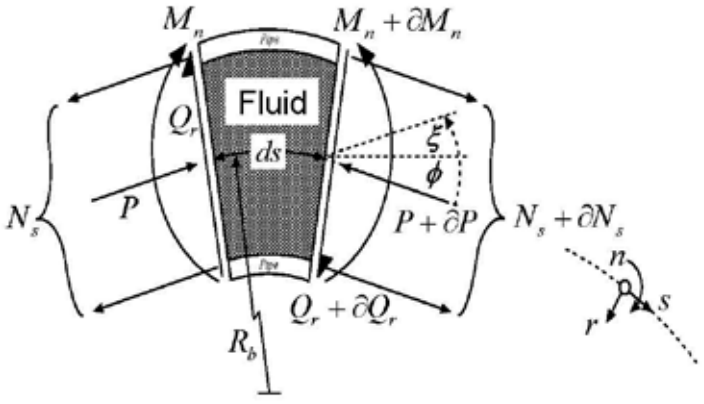

Figure 1 Sign convention for pipe element

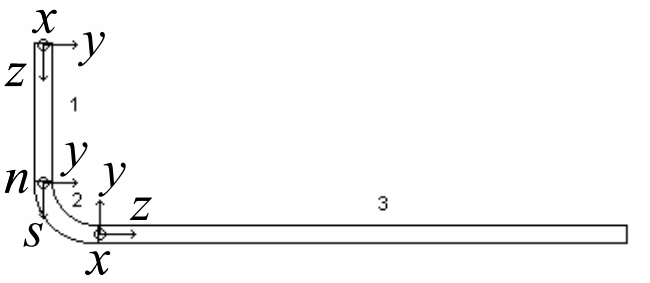

Figure 2 Pipe component numbering and coordinate systems

The discrete pipe bend model is given by Equations (9) – (18). The superscripts refer to the pipe component ("component") numbering given in Figure 2 below. The variables shown are equivalent to their continuous pipe bend counterparts, except for a coordinate system change.

$$A_f(V^1 - \dot{u}_z^1) = A_f(V^3 - \dot{u}_z^3) \qquad P^1 = P^3 \qquad (9),(10)$$

$$\dot{u}_z^1 = \dot{u}_y^3 \qquad A_f P^1 - A_p \sigma_z^1 = Q_y^3 \qquad (11),(12)$$

$$\dot{u}_y^1 = -\dot{u}_z^3 \qquad -Q_y^1 = A_f P^3 - A_p \sigma_z^3 \qquad (13),(14)$$

$$\dot{\theta}_z^1 = \dot{\theta}_z^3 \qquad M_z^1 = M_z^3 \qquad (15),(16)$$

The boundary condition for the excitation end (component 1) is given by Equations (17) – (20). Note that Equation (18) is the source of the system excitation. The boundary condition for the opposite end also consists of Equations (17) – (20) bar the $F_{excitation}$ term in Equation (18). The component joint conditions simply consisted of equating the respective state variables.

$$V^1 = \dot{u}_z^1 \qquad A_f P^1 + F_{excitation} = A_p \sigma_z^1 - m\ddot{u}_z^1 \qquad (17),(18)$$

$$Q_y^1 = 0 \qquad M_x^1 = 0 \qquad (19),(20)$$

For experimental reasons, this study is concerned with the following state variables: P, $a_{z,s}$ (axial acceleration) and $a_{y,r}$ (transverse acceleration).

Solving for the unknowns

In order to solve the system of PDEs above, the spectral method is used. This allows for frequency domain information to be extracted in addition to providing a time domain solution. The method involves (1) obtaining the frequency or "spectral" representation of the force input, $\hat{F}(\omega)$, by applying the forward Fourier Transform (FFT), (2) obtaining the system transfer function, $\hat{H}(\omega)$ from theory, (3) multiplying the two, and (4) applying the inverse Fourier Transform (IFT) to the result. In other words,

$$\text{solution at } (z,t) = \text{IFT}\left[\hat{H}(\omega)\cdot\left\{\text{FT}\left[F(z,t)\right]\right\}\right] \qquad (21)$$

In order to obtain $\hat{H}(\omega)$, each state variable is expressed in a similar form to that shown below, in which $\hat{u}_n(\omega_n)$ is the amplitude spectrum:

$$\dot{u}(z,t) = \sum_n \hat{u}_n(\omega_n) e^{i\omega_n t} \qquad (22)$$

The benefit of this representation is that time derivatives of differential equations can be replaced by quasi-algebraic spectral expressions:

$$\frac{\partial \dot{u}}{\partial t} = \sum_n i\omega \hat{u}_n e^{i\omega t} \qquad \frac{\partial^m \dot{u}}{\partial t^m} = \sum_n i^m \omega^m \hat{u}_n e^{i\omega t} \qquad (23,\ 24)$$

If we also express $\hat{u}(z,\omega) = u_0 e^{-ikz}$, and substitute this equation and the forms given by Equations (23) and (24) for every state variable into the PDEs above, then a set of simultaneous equations is obtained in which $\boldsymbol{MX} = 0$, where $\boldsymbol{X}$ is a vector of the amplitude coefficients (e.g. u_0) and $\boldsymbol{M}$ is a matrix of the coefficients of the simultaneous equations (i.e. constants, i,ω,k). Hence, $\boldsymbol{MX} = 0$. This is only possible if

$$\det[\boldsymbol{M}] = 0 \qquad (25)$$

The above equation will yield a polynomial which enables us to determine the quantity and form of the wavenumbers, k.

In order to solve for the amplitude coefficients, one needs to look at the boundary and component joint conditions of the system. But first, the equations which represent the response of each state variable need to be set-up for each pipe component in the system. For example, for component 1, the full response for the fluid pressure is given by:

$$\hat{P}^1(z,\omega) = P_1^1 e^{-ik_1 z} + P_2^1 e^{-ik_2 z} + P_3^1 e^{ik_1 z} + P_4^1 e^{ik_2 z} \qquad (26)$$

The number of modes or waves is determined by the quantity of wavenumbers solved above. For the pressure here, there are 4 waves in total: 2 propagating waves in both the forward and backward directions. Once these state variable equations are input into the boundary and joint component conditions, the algebraic relationships between the various amplitude coefficients for a particular mode (e.g. $V_1 = f(P_1)$) together with the result enable these coefficients to be determined. That is, if $\boldsymbol{B}$ is the boundary and component joint condition matrix, $\hat{\boldsymbol{F}}$ is the spectral form of the force history and $\boldsymbol{C}$ is the coefficient matrix, then $C = B^{-1}\hat{F}$ and $B^{-1} = \hat{H}(\omega)$. This then permits a time domain solution through use of the IFT.

2. EXPERIMENT DESIGN

An impact hammer was chosen as the means to excite the system experimentally. This was for a number of reasons:

- an impact hammer produces a "pulse" excitation which is often clearly identifiable in time domain histories;
- use of an impact hammer meant that the force could be measured directly and easily;
- this method of excitation meant that the end of the pipe which the hammer struck was simple. The associated modelling of this end meant that discrepancies between theory and experiment would be minimised;
- mounting the large impact hammer in a pendulum-like manner meant that the experiment was reproducible and was not overly complicated.

In order to prevent cavitation occurring within the pipe, the fluid was statically pressurised to 500 kPa.

Because this study attempts to compare theory with experiment, 3 state variables which adequately capture the response of the fluid, pipe axial motion and pipe transverse motion were deemed to be sufficient. Hence, only the following measurements were accounted for: P, $a_{z,s}$ and $a_{y,r}$. These variables allowed a suitable comparison between the predictions given by

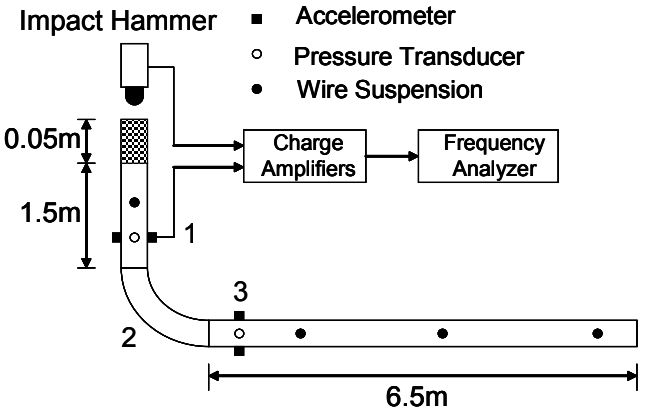

Figure 3 Experimental set-up

the theory and the actuality of the experimental results.

A schematic of the rig can be seen in Figure 3. A force measurement taken from the transducer in the impact hammer is used to input into the theoretical models via Equation (18). The physical properties of the materials involved and the experimental design parameters are listed in Table 1. Details of the pipe components, pendulum impact-hammer and a cross section where the pressure and acceleration sensors are mounted are shown in Figure 4.

Pipe (black steel)		Liquid (water)
$L_1 = 1.5$ m	$E = 210$ Gpa	K $= 2.2$ Gpa
$L_3 = 6.5$ m	$\rho_p = 7850$ kg/m^3	$P_f = 1000$kg/m^3
$R_b = 0.152$ m	$\upsilon = 0.29$	$P_0 = 500$ kPa
$R_p = 0.03485$ m	$m_1 = 2.06$ kg	
$T = 0.0032$ m	$m_3 = 0.1114$ kg	

Table 1 Physical properties and some design parameters

Measurements were taken from two positions located 0.725 m from either side of the pipe bend joints. This distance ensured that all higher-order evanescent modes were negligible.

Dimensional sizing

In studies such as this one, non-dimensional frequency values are often quoted because of the inherent connection between frequency and system lengths. That is, increasing the excitation frequency is equivalent to decreasing the characteristic length of the system and vice versa. Non-dimensional frequencies are not used here. However, we do quote two important values that fulfil the same function. The ring frequency, f_{ring}, is approximately 24 kHz. Additionally, the ratio of the bend radius to pipe radius is approximately 4.4. Above the ring frequency, the response of the pipe is similar to that of a flat thin plate, while below it the response is more complex due to the shell wall curvature [11]. The R_b/R_p ratio characterises the size of the pipe bend: a large value indicates the pipe bend is 'sweeping' while a small value indicates a 'stubby' pipe bend.

3. RESULTS AND DISCUSSION

A power spectrum of a typical strike from the impact hammer is shown in Figure 5. Note the narrow band of significant frequencies (< 1 kHz).

The theoretical time domain responses predicted by both bend models are shown in Figure 6 and Figure 8. Experimental time histories and the theoretical predictions using the continuous bend model are shown in Figure 7 and Figure 9. The results are plotted separately to improve the clarity of the results. Note that the time window is only very short in both sets of figures. This is also to increase the clarity of the results.

In general, there is not a significant difference between the predictions of the two models. The fact that the discrete model does not adequately account for the size and mass of the bend does not seem to have a dramatic effect on the quality of the prediction in the frequency range of interests. There are, however, some minor

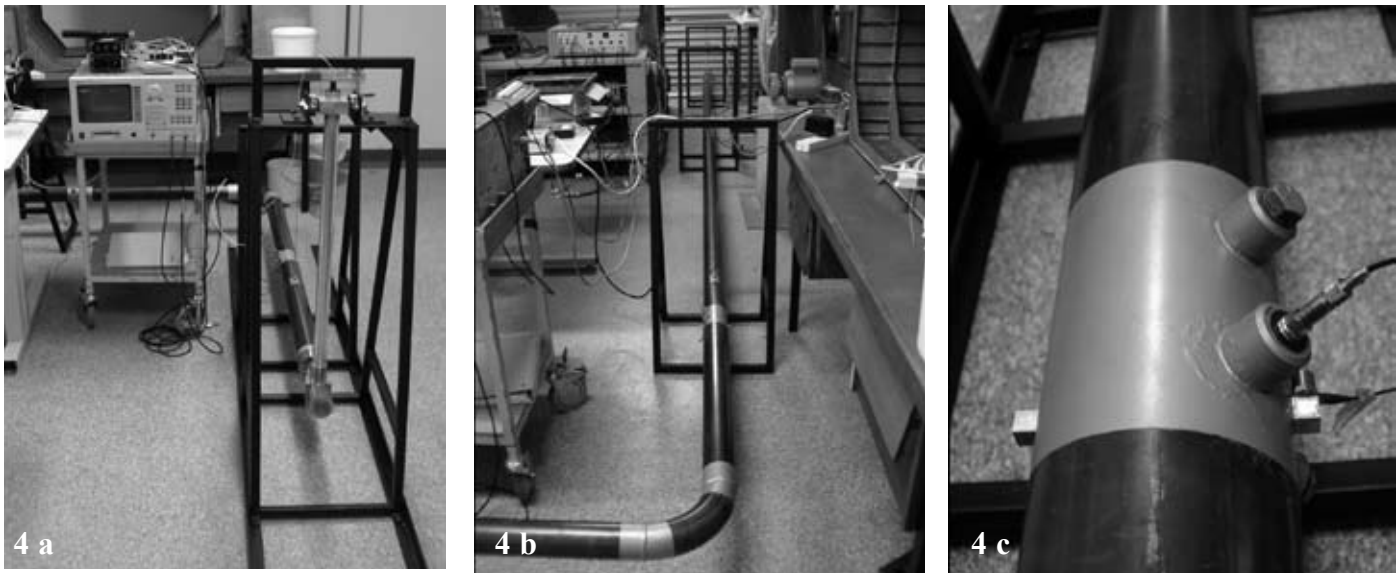

Figure 4 Photographs of experimental set-up (a) data acquisition equipment, pendulum impact-hammer and pipe component 1; (b) pipe component 2 and supports; (c) cross-section of sensor positions, pressure transducer and cube-mounted accelerometer shown

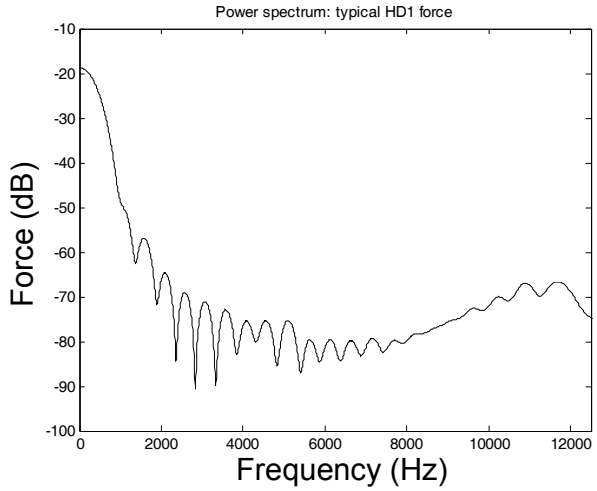

Figure 5 Power spectrum of typical strike from the impact hammer

discrepancies with the transverse accelerations given in Figure 6 and Figure 8. It is interesting to note that such discrepancies are not found with the pressure and axial acceleration. The power spectrum of the transverse accelerations (not shown) actually shows appreciable magnitudes past 5 kHz. Because of this fact, one expects there to be discrepancies between the two models as they are only equivalent in the low frequency ranges.

Furthermore, the theory predicts the response of the system somewhat accurately. For both pressure and axial acceleration measurements, the theory performs reasonably well. However, for the transverse acceleration, there are discrepancies that are different in nature to those shown for the theoretical comparisons. Here the continuous model consistently leads the experimental measurement. This indicates that the waves in the real system are actually travelling slower. A reasonable explanation for this is the fact that the pipe is subject to a complicated pre-stress as a result of the static pressure and fluid loading. A component of this stress might be axial pre-compression, which decreases the speed of travelling waves. Although the effect of axial pre-stress on the speed of transverse wave in beams has been studied [12], further study on this effect in pipeline systems will still have some practical value.

Discrepancy other than the time lags may be due to the limitation of the modelling of the experimental rig by using the in-plane components. The circumferential distribution of transverse waves in practical pipes may be 'polarised' [13] in directions other than in parallel or perpendicular to the (y, z) plane of the pipe coordinates (as defined in Figure 2). As a result, the measured transverse wave response in the (y, z) plane may be contributed by both in-plane and out-of-plane transverse wave components. For this case, both components have two nodes in the circumferential direction. Modelling of the interaction between the in-plane pressure/axial waves with in-plane and out-of-plane transverse waves at pipe bends requires the use of a 3-dimensional pipeline model and experimental determination of the polarization angle of the circumferential modes of the transverse waves.

Although this work concentrates on the measurement and modelling of transient pressure and vibration waves in fluid-filled pipes with bends, the methods can be used to evaluate the acoustical energy transmission and energy exchange between

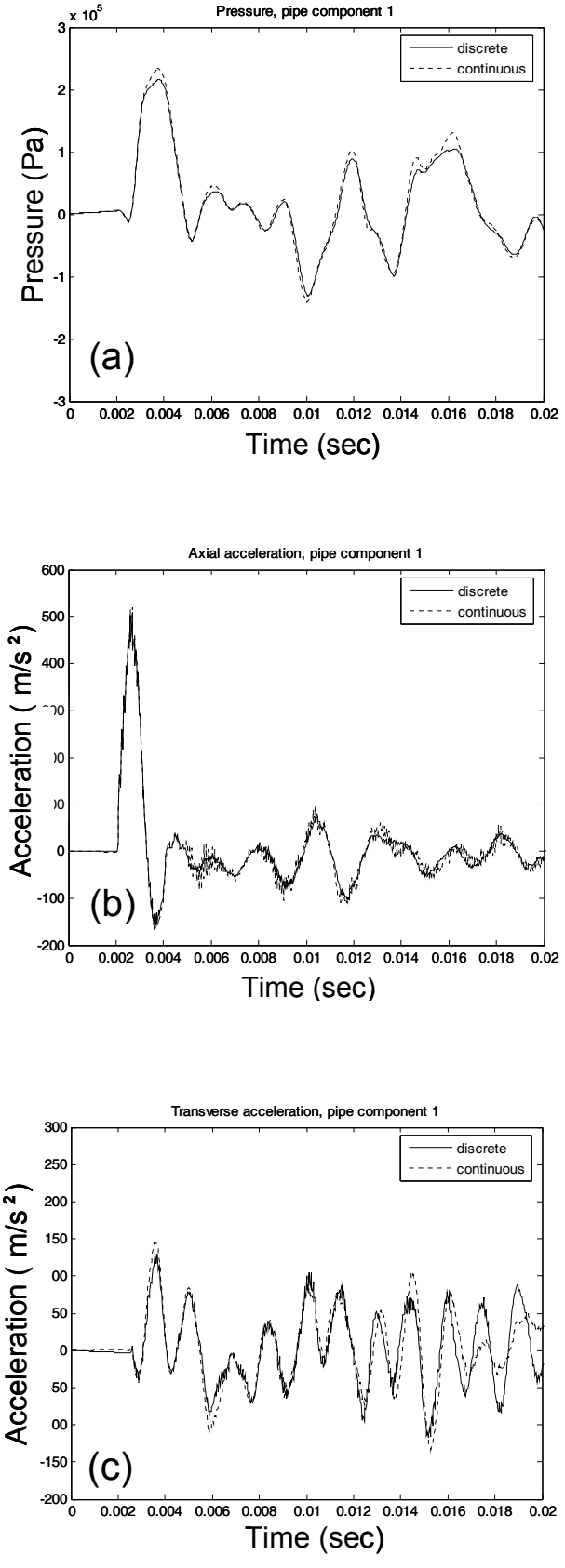

Figure 6 Time domain responses, discrete versus continuous bend models, HD1 typical impact (top to bottom): (a) pressure, pipe component 1; (b) axial acceleration, pipe component 1; (c) transverse acceleration, pipe component 1

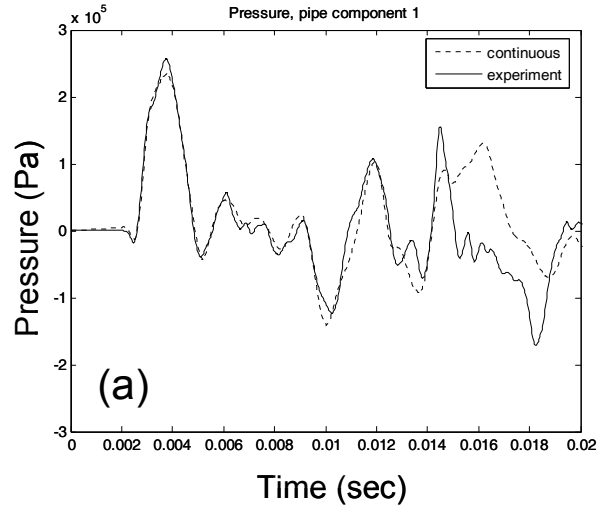

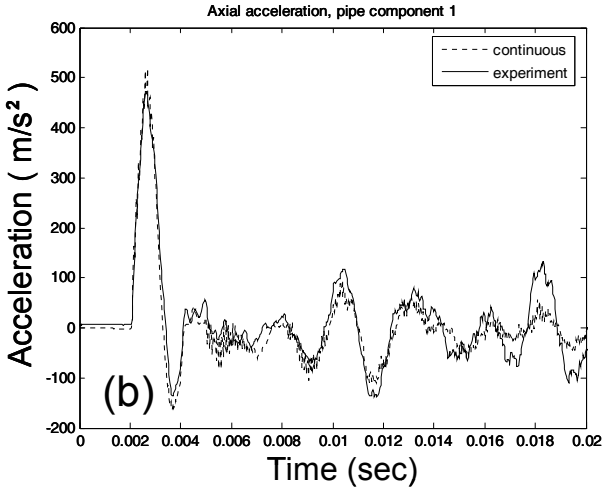

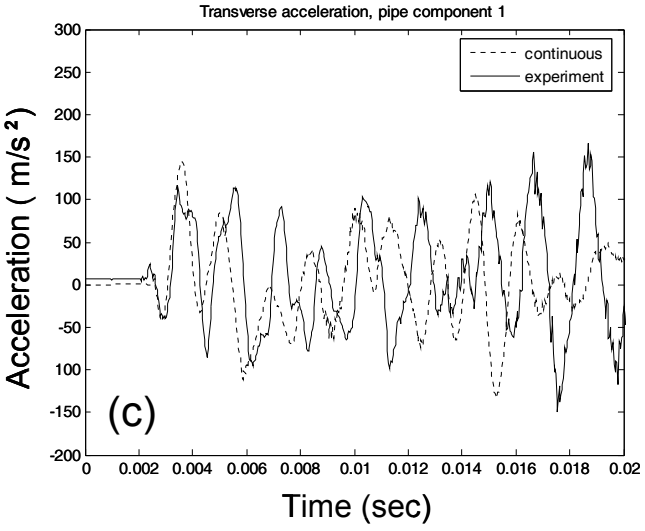

Figure 7 Time domain responses, experimental versus continuous bend models, HD1 typical impact (top to bottom): (a) pressure, pipe component 1; (b) axial acceleration, pipe component 1; (c) transverse acceleration, pipe component 1. All acceleration measurements have been filtered by an analog low-pass filter with a cut-off frequency of 10 kHz

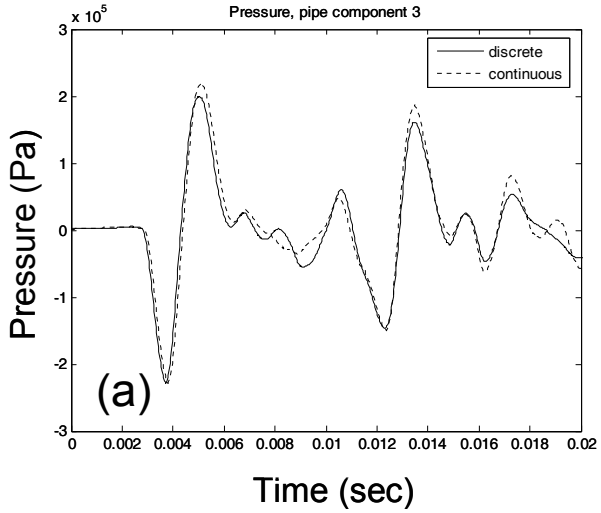

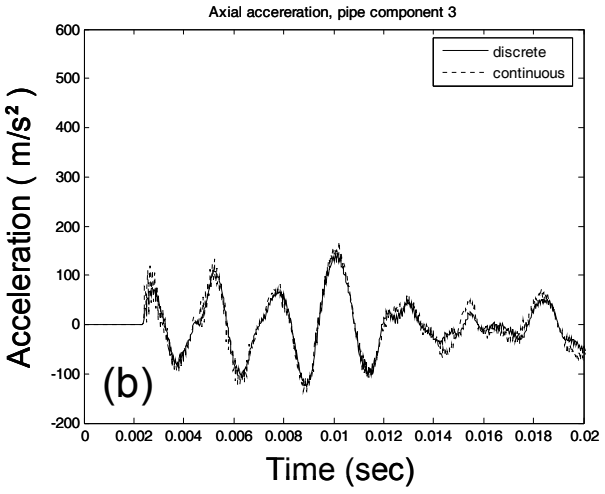

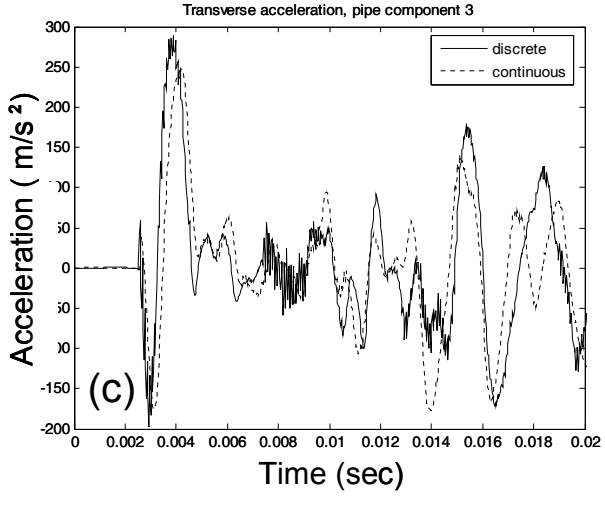

Figure 8 Time domain responses, discrete versus continuous bend models, HD1 typical impact (top to bottom): (a) pressure, pipe component 3; (b) axial acceleration, pipe component 3; (c) transverse acceleration, pipe component 3

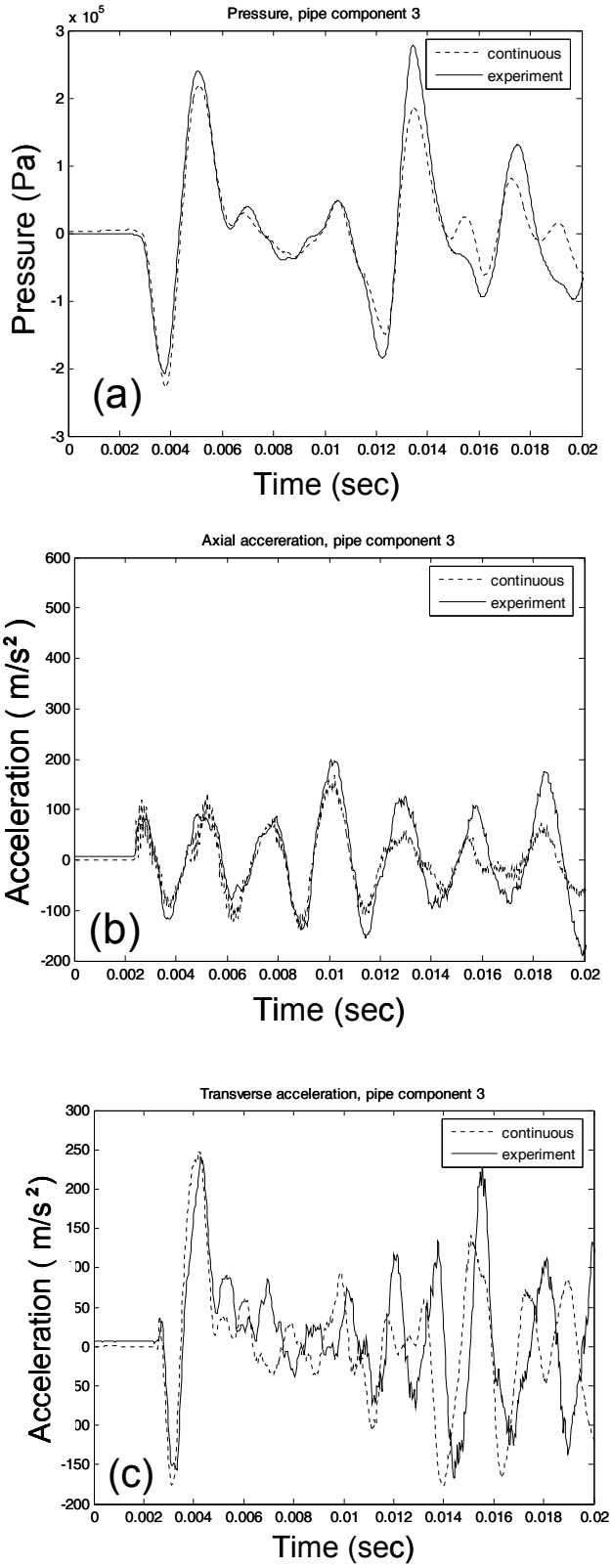

Figure 9 Time domain responses, experimental versus continuous bend models, HD1 typical impact (top to bottom): (a) pressure, pipe component 3; (b) axial acceleration, pipe component 3; (c) transverse acceleration, pipe component 3; All acceleration measurements have been filtered by an analog low-pass filter with a cut-off frequency of 10 kHz

different wave types at the pipe bends. Ultimately, the energy distributions in different part of pipelines and carried by different wave types are responsible to the noise emission from and dynamic stress concentration in pipes, which are important information for pipeline design and maintenance.

4. CONCLUSIONS

This study compared the theoretical predictions of two different bend models of an L-shaped, water-filled pipe system with measurements taken from an experimental rig. The results show that for a broad impulse consisting of significant frequencies up to 1 kHz ($f_{\text{ring}} \approx 24$ kHz, $R_b/R_p \approx 4.4$), the discrete bend model is superior to the continuous model due to computational efficiency. Future work will consist of repeating the analysis here but for higher excitation frequencies. It is important to determine when the accuracy of the two models disagrees.

ACKNOWLEDGEMENTS

Support for this work from the Australian Research Council and SVT Engineering Consultants is gratefully acknowledged. We also thank the reviewers and editor for their useful comments.

REFERENCES

[1] A. F. D'Souza and R. Oldenburger, "Dynamic Response of Fluid Lines", *ASME Journal of Basic Engineering*, **86**, 589-598 (1964)

[2] L. C. Davidson and J. E. Smith, "Liquid-Structure Coupling in Curved Pipes", *The Shock and Vibration Bulletin*, **40(4)**, 197-207 (1969)

[3] L. C. Davidson and D. R. Samsury, "Liquid-Structure Coupling in Curved Pipes − II", *The Shock and Vibration Bulletin*, **42**(1), 123-136 (1972)

[4] F. J. Hatfield, L. C. Davidson and D. C. Wiggert, "Acoustic Analysis of Liquid-Filled Piping by Component Synthesis: Experimental Validation and Examination of Assumptions", *ASME-PVP Fluid Transients and Fluid-Structure Interaction*, **64**, 106-115 (1982)

[5] D. J. Wood and S. P. Chao, "Effect of pipeline junctions on waterhammer surges", *ASCE Transportation Engineering Journal,* **97**, 441-456 (1971)

[6] D. H. Wilkinson, "Acoustic and Mechanical Vibrations in Liquid-Filled Pipework Systems", in *BNES International Conference on Vibration in Nuclear Plant*, British Nuclear Energy Society, Keswick, U.K., 863-878 (1978)

[7] R. A. Valentin, J. W. Phillips and J. S. Walker, "Reflection and Transmission of Fluid Transients at an Elbow", in *Transactions of SMiRT5*, International Association for Structural Mechanics in Reactor Technology, Berlin, Germany, (1979)

[8] M. W. Lesmez, D. C. Wiggert and F. J. Hatfield, "Modal Analysis of Vibrations in Liquid-Filled Piping Systems', *ASME Journal of Fluids Engineering*, **112**, 311-318 (1990)

[9] A. S. Tijsseling, A. E. Vardy and D. Fan, "Fluid-Structure Interaction and Cavitation in a Single-Elbow Pipe System", *Journal of Fluids and Structures,* **10**, 395-420 (1996)

[10] A. E. Vardy, D. Fan and A. S. Tijsseling, "Fluid-Structure Interaction in a T-Piece Pipe", *Journal of Fluids and Structures*, **10**, 763-786 (1996)

[11] C. R. Fuller, "The Effects of Wall Dis continuities on the Propagation of Flexural Waves in Cylindrical Shells", *Journal of Sound and Vibration*, **75**(2), 207-228 (1981)

[12] K. F. Graff, "Wave Motion in Elastic Solid", Clarendon, Oxford, (1975)

[13] R. S. Ming, J. Pan and M. P. Norton, "The measurement of structure-borne sound energy flow in an elastic cylindrical shell", *J. Sound & Vib.*, **242**(4), 719-735 (2001)